

IAC-19-C1.1.10

LOW-THRUST TRAJECTORY DESIGN FOR A CISLUNAR CUBE_{SAT} LEVERAGING STRUCTURES FROM THE BICIRCULAR RESTRICTED FOUR-BODY PROBLEM

Robert Pritchett

Purdue University, USA, pritcher@purdue.edu

Kathleen C. Howell

Purdue University, USA, howell@purdue.edu

David C. Folta

NASA Goddard Space Flight Center, USA, david.c.folta@nasa.gov

The upcoming Lunar IceCube (LIC) mission will deliver a 6U CubeSat to a low lunar orbit via a ride-share opportunity during NASA's Artemis 1 mission. This presents a challenging trajectory design scenario, as the vast change in energy required to transfer from the initial deployment state to the destination orbit is compounded by the limitations of the LIC's low-thrust engine. This investigation addresses these challenges by developing a trajectory design framework that utilizes dynamical structures available in the Bicircular Restricted Four-Body Problem (BCR4BP), along with a robust direct collocation algorithm. Maps are created that expedite the selection of invariant manifold paths from a periodic staging orbit in the BCR4BP, as these offer favorable connections between the LIC transfer phases. Initial guesses assembled from these maps are passed to a direct collocation algorithm that corrects them in the BCR4BP while including the variable low-thrust acceleration of the spacecraft engine. Results indicate that the ordered motion provided by the BCR4BP and the robustness of direct collocation combine to offer an efficient and adaptable framework for designing a baseline trajectory for the LIC mission.

1. INTRODUCTION

Advances in spacecraft technology miniaturization and an increase in launch opportunities have exponentially increased the number of CubeSats launched in the two decades since the platform was first proposed. Early success has motivated concept development for CubeSat missions beyond the bounds of low Earth orbit (LEO). In 2018, the two MarCO Cubesats, as the first to operate beyond Earth orbit, were deployed at Mars to monitor the entry, descent, and landing of the *Insight* lander.¹ Soon, thirteen CubeSats will utilize a rideshare opportunity on the Space Launch System (SLS) during the Artemis 1 mission to reach a variety of destinations well beyond LEO. Several of these spacecraft will reach heliocentric space, including the Near Earth Asteroid Scout (NEA Scout) and the CubeSat for Solar Particles (CuSP), which will fly by a near-Earth asteroid and investigate space weather, respectively. Other CubeSats on this launch which are destined for the Moon, include Lunar IceCube, Lunar Flashlight, and LunaH-Map. Together, these far-flung CubeSat missions indicate that small spacecraft will play an increasingly important role in space exploration.

While the CubeSat revolution has opened exciting opportunities, it brings new challenges. Despite technological advancements, ambitious CubeSat missions often require “doing more with less”. For mission design, innovative trajectory design approaches are necessary that fully exploit natural dynamics. The Lunar IceCube (LIC) concept offers an excellent example of the challenges. This mission will deliver a 6U CubeSat to a low lunar orbit (LLO) where LIC will collect data on water transport throughout the lunar surface. A challenging trajectory design scenario emerges, as the vast change in energy required to transfer from the initial deployment state to LLO is compounded by the limited control authority of the LIC low-thrust engine. Furthermore, as a secondary payload, LIC is subject to changes in launch date and conditions required by the primary mission. These challenges necessitate a trajectory design strategy that is flexible and incorporates natural forces to assist with the required energy change.

This investigation proposes a trajectory design framework that addresses the challenges of the Lunar IceCube mission by utilizing dynamical structures available in the Bicircular Restricted Four-Body Problem (BCR4BP) along with a robust direct col-

location algorithm. Designing in the BCR4BP enables the gravitational force of the Sun to be leveraged to achieve part of the required energy change, while avoiding the additional perturbations of a full ephemeris model. A key feature of the proposed design approach is the use of a staging orbit near the Moon to split the trajectory into two phases: the first from spacecraft deployment to the staging orbit, and the second from the staging orbit to the science orbit. This choice allows the two halves of the LIC trajectory to be designed mostly independently, thus, simplifying the redesign process if deployment conditions change. Moreover, a periodic orbit in the BCR4BP is employed as the staging orbit, to leverage its invariant manifolds for the design of efficient paths to and from the staging orbit. Another crucial component of the proposed framework is a direct collocation algorithm to correct initial guesses developed in the BCR4BP into optimal low-thrust trajectories. The robust convergence properties of direct collocation facilitate a wider variety of initial guesses despite large discontinuities in states or time. Together, these key design choices produce a design process that directly addresses the challenges of the Lunar IceCube mission. After an overview of the necessary background, the proposed trajectory design framework is described. Sample Lunar IceCube trajectories are constructed with the proposed strategies. While the trajectory design procedure is applied to the Lunar IceCube mission, it is sufficiently general for a wide variety of low-thrust missions especially those with limited control authority.

2. BACKGROUND

2.1 Previous Work

First proposed in 2015, the Lunar IceCube (LIC) mission is a collaborative effort led by Morehead State University and supported by Goddard Space Flight Center (GSFC), Busek, and Catholic University of America². During this mission the presence and movement of water in all its forms across a broad swath of the lunar surface is to be investigated. To enable the science collection, the 6U CubeSat will conduct science operations in a low lunar orbit (LLO) that covers a range of longitudes on the sunlit side of the Moon with a perilune altitude of 100 km. The full set of Keplerian orbital elements that define the science orbit are provided in Table 1 and are driven by the science requirements as well as the desire to maximize spacecraft lifetime while minimizing the station-keeping cost.³ Station-keeping and the transfer trajectory to the science orbit are achieved via

Table 1: Lunar IceCube science orbit Keplerian orbital elements defined in a Moon-centered inertial frame. Inclination is measured relative to the Moon’s equator and the right ascension of the ascending node (RAAN) is defined with respect to the vernal equinox vector.

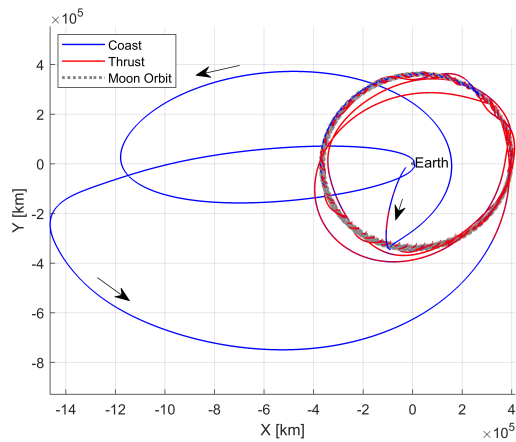
Orbital Element	Value
Semi-Major Axis, a	4271.4 km
Eccentricity, e	0.5697
Inclination, i	89.35°
RAAN, Ω	65°
Argument of Periapsis, ω	355°

a BIT-3 Busek ion thruster, which is capable of a maximum thrust of 1.24 mN, a specific impulse (I_{sp}) of 2640 seconds, and storing up to 1.5 kg of propellant.⁴ Given the total 14 kg mass of LIC, these engine characteristics equip it with a maximum acceleration of $8.857 \times 10^{-5} \text{ m/s}^2$. This value is compared to the maximum acceleration values of several other low-thrust spacecraft in Table 2; the low-thrust capability of LIC is clearly of the same order of magnitude as other recent or proposed low-thrust missions. The mission design challenge for LIC is due less to

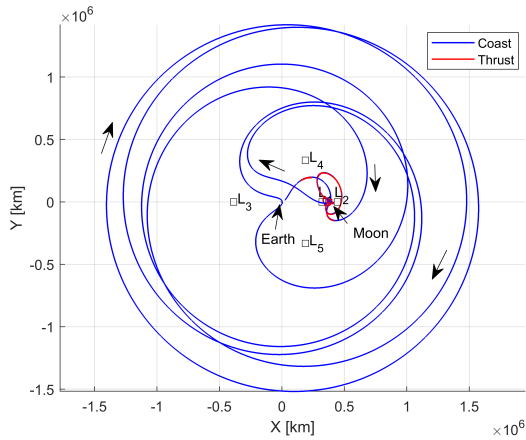
Table 2: Representative low-thrust spacecraft acceleration levels.

Spacecraft	Max Acceleration (m/s^2)
Deep Space 1 ⁵	1.892×10^{-4}
Lunar IceCube	8.857×10^{-5}
Dawn ⁶	7.473×10^{-5}
Gateway ⁷	3×10^{-5}

the small thrust magnitude and more to the fact that this engine must deliver a massive change in energy to transfer from the high-energy deployment state near the Earth to the low-energy LLO. While the initial velocity of LIC relative to the Earth is less than escape velocity, the subsequent ballistic path includes a flyby of the Moon that causes LIC to escape the Earth-Moon system. Low-thrust maneuvers must be initiated shortly after deployment to prevent escape from occurring. In contrast to this high-energy deployment, the LIC science orbit possesses an energy low enough that the spacecraft is securely captured at the Moon. Despite the challenge of achieving this large change in energy, engineers at GSFC have developed a complete baseline trajectory, plotted in Figure 1, that utilizes the current launch date of June 25th 2020. However, this baseline trajectory must be



(a) Earth-Centered J2000 Inertial Frame



(b) Earth-Moon Rotating Frame

Fig. 1: Current baseline for Lunar IceCube trajectory developed assuming a June 25th, 2020 launch date.

redesigned when an updated launch date is released in the near future. Previous experience has demonstrated that varying the launch date can significantly impact the geometry of the LIC trajectory.

Faced with a challenging trajectory design scenario and uncertain launch conditions, engineers at GSFC have been informed by the results of several investigations on LIC trajectory design. A strategy that utilizes the high-fidelity General Mission Analysis Tool (GMAT) to design an LIC trajectory with a capture orbit at the Moon is offered by Mathur⁸. An innovative design approach for LIC is also presented by Bosanac, Folta, Cox, and Howell which subdivides the Lunar IceCube trajectory into three phases: deployment, phasing and energy adjustment, and lunar capture. A strategy for linking these phases that

incorporates periapse maps and phasing arcs generated in the Sun-Earth Circular Restricted Three-Body Problem (CR3BP) or the BCR4BP is developed by Bosanac et al.^{9–11}. Particular focus on the dynamics of the lunar capture phase is delivered separately by Folta et al.¹². The strategy presented by Bosanac et al. is effective, and the current investigation expands upon their work by approaching the design problem with a framework that utilizes BCR4BP dynamical structures and direct collocation. This application may yield a design procedure that requires less computational time and is more robust with poor initial guesses.

In addition to work focused on LIC, this investigation is influenced by a greater body of literature on leveraging the influence of the Sun to design transfers from the Earth to the Moon. Belbruno and Miller demonstrate new types of Earth to Moon trajectories by simultaneously incorporating the gravitational influence of the Sun in addition to the Earth and Moon. Strategies for utilizing this acceleration to develop low-energy trajectories from the Earth to the Moon are developed by many authors, including Koon et al.¹³, Gómez et al.¹⁴, as well as Parker and Martin¹⁵. Low-energy trajectory design techniques are also applied to design low-thrust trajectories to the Moon by Mingotti et al.¹⁶ and Zanuttera et al.¹⁷. The present work uses direct collocation to compute low-thrust transfers building on the work of authors such as Enright and Conway¹⁸ as well as Grebow, Ozimek, and Howell¹⁹ who also employ this algorithm to generate low-thrust Earth to Moon transfers. Perez-Palau and Epenoy explore similar transfers using an indirect optimal control approach in a four-body dynamical model²⁰. Some authors exploring low-energy trajectory design also demonstrate transfers from Earth-Moon halo orbits to LLO, a strategy used in this investigation. Parker and Anderson²¹ offer an impulsive transfer, while Mingotti et al. demonstrate a low-thrust result²². Recently, Cheng et al.²³ and Cao et al.²⁴ have more closely examined impulsive transfers from halo orbits to LLO in the CR3BP.

2.2 Bicircular Restricted Four-Body Problem

The BCR4BP builds on the assumptions of the CR3BP. The CR3BP models the path of a third body, P_3 , under the influence of two more massive primary bodies, P_1 and P_2 . These bodies are assumed to follow circular Keplerian orbits about their mutual barycenter, B_1 . Additionally, the third body is assumed to possess negligible mass in comparison to the primary bodies, and this assumption is reason-

able when the mass of the third body is quite small, e.g., a spacecraft. Finally, the mass ratio of P_1 and P_2 is denoted, $\mu = \frac{m_2}{m_1+m_2}$, and is used to characterize the CR3BP system.

The BCR4BP assumes the addition of a fourth body, P_4 ; both P_4 and the P_1 - P_2 barycenter, B_1 , move in circular orbits about their mutual barycenter, B_2 . In this investigation, P_4 is always the Sun, thus the mass of P_4 equals the mass of the Sun, m_S . The circular orbits of P_1 and P_2 are not affected by the gravitational force of the Sun. As a result of this assumption, the BCR4BP is *not coherent* because the motion of P_1 and P_2 are not influenced by the Sun, i.e., the indirect effects of the Sun are not incorporated. Additionally, as in the CR3BP, the mass of P_3 is assumed to be negligible relative to the other three bodies, i.e., $m_3 \ll m_2 < m_1 < m_S$. In general, the BCR4BP does not require that the Sun- B_1 orbit be coplanar with the P_1 - P_2 orbit; however, in this investigation a coplanar model is employed. This model as well as a non-coplanar formulation are presented by Boudad²⁵.

It is insightful to examine motion in the BCR4BP from the perspective of two different rotating reference frames. The first is a reference frame rotating with P_1 and P_2 , whose axes are defined by three orthogonal unit vectors. By convention, the \hat{x} unit vector of this frame points from P_1 to P_2 , while the \hat{z} unit vector is parallel to the angular momentum vector of P_2 about P_1 . Finally, the \hat{y} unit vector is defined to complete the orthonormal set. A similar second rotating reference frame is defined for the Sun and B_1 , but the \hat{x}' unit vector is instead in the direction of B_1 from the Sun. Quantities expressed in the Sun- B_1 rotating frame are generally denoted with an apostrophe, e.g., x' is the x position coordinate of P_3 in the Sun- B_1 rotating frame. When the coplanar assumption is made, the orbit of the Sun as viewed from the P_1 - P_2 rotating frame is modeled as illustrated in Figure 2. The position of the Sun in the P_1 - P_2 rotating frame is determined by the Sun angle, θ_S , and the distance from B_1 to the Sun is defined by the constant value a_S . Viewed from this frame, the Sun rotates clockwise about B_1 , thus the value of θ_S decreases with time.

Motion in the BCR4BP is described by a set of differential equations similar to those of the CR3BP, but modified to accommodate the perturbing acceleration of the Sun. The P_1 - P_2 rotating frame together with the Sun- B_1 rotating frame are commonly employed for analysis in the BCR4BP, and the equations of motion for P_3 may be expressed in either of these

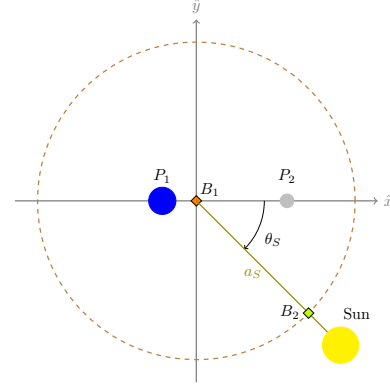


Fig. 2: Definition of the Sun angle in the Bicircular Restricted Four-Body Problem.

frames. The equations of motion for P_3 , expressed in the P_1 - P_2 frame and including a low-thrust force, are,

$$\ddot{x} = 2\dot{y} + \frac{\partial \Psi}{\partial x} + \frac{T_x}{m} \quad (1)$$

$$\ddot{y} = -2\dot{x} + \frac{\partial \Psi}{\partial y} + \frac{T_y}{m} \quad (2)$$

$$\ddot{z} = \frac{\partial \Psi}{\partial z} + \frac{T_z}{m} \quad (3)$$

$$\dot{m} = \frac{T}{v_e} \quad (4)$$

where the low-thrust force is represented by the three components of the thrust vector $\mathbf{T} = \{T_x \ T_y \ T_z\}$, and $\|\mathbf{T}\| = T$. The magnitude of the thrust vector appears in Equation 4, along with the exhaust velocity, v_e . Together these parameters define the mass flow rate of the spacecraft, \dot{m} . Additionally, Ψ is the system pseudo-potential written in terms of P_1 - P_2 rotating frames coordinates. This pseudo-potential and the pseudo-potential as expressed in Sun- B_1 coordinates, Ψ' , are,

$$\Psi = \frac{1-\mu}{r_{13}} + \frac{\mu}{r_{23}} + \frac{1}{2}(x^2 + y^2) + \frac{m_S}{r_{S3}} - \frac{m_S}{a_S^3}(x_S x + y_S y + z_S z) \quad (5)$$

$$\Psi' = \frac{1}{2}(x'^2 + y'^2) + \frac{1-\mu_{SB1}}{r'_{S3}} + \frac{\mu_{SB1}(1-\mu_{P1P2})}{r'_{13}} + \frac{\mu_{SB1}\mu_{P1P2}}{r'_{23}} \quad (6)$$

where the distance from the Sun to P_3 is represented by r_{S3} , and μ_{SB1} is the mass ratio of the Sun- B_1 system. Together these equations govern motion in the BCR4BP.

To facilitate numerical computation, the dependent variables in this dynamical model are nondimensionalized via a set of characteristic quantities. The values of the characteristic quantities are determined by the frame that the states are expressed in. When states are expressed in the P_1 - P_2 rotating frame the characteristic length, l^* , is defined as the distance between P_1 and P_2 ; the characteristic mass, m^* , is equal to the combined mass of P_1 and P_2 ; and the characteristic time is determined such that the nondimensional angular velocity of P_1 and P_2 is equal to one. The characteristic quantities are defined similarly when states are expressed in the Sun- B_1 rotating frame, except that the parameters of the Sun and B_1 replace those of P_1 and P_2 in the previous case. In this investigation, numerical propagation is performed using the equations of motion expressed in the P_1 - P_2 rotating frame.

In contrast to the CR3BP, the BCR4BP is not an autonomous system, i.e., motion in this model is time dependent. As a consequence, this system possesses no integral of the motion. However, the Hamiltonian, serves as a useful metric for analyzing the motion of P_3 in the BCR4BP. The Hamiltonian defined in this investigation does not include the low-thrust force, thus it represents only the ballistic energy of the system. The Hamiltonian may be computed using coordinates expressed in either the P_1 - P_2 or Sun- B_1 rotating frames.

$$H = 2\Psi - (\dot{x}^2 + \dot{y}^2 + \dot{z}^2) - \sigma \quad (7)$$

$$H' = 2\Psi' - (\dot{x}'^2 + \dot{y}'^2 + \dot{z}'^2) \quad (8)$$

The value of H is scaled by a constant parameter σ that is incorporated to offset the high value terms introduced by the Sun and ensure that H is of a similar magnitude to the Jacobi constant value of the Earth-Moon CR3BP. Throughout this analysis, $\sigma = 1690$ nondimensional units.

The same types of dynamical structures that are available in the CR3BP also emerge in the BCR4BP, namely, periodic and quasi-periodic orbits as well as their invariant manifolds. Because the BCR4BP is non-autonomous, these structures are not only defined by position and velocity states, but also by specific epochs, i.e., Sun angles. A periodic orbit in the BCR4BP requires a repetition of the same position and velocity states at the same Sun angle. This angle requirement implies that all periodic orbits in the Sun-Earth-Moon BCR4BP possess a resonance with the synodic period of the Sun, approximately 29.5 days. The Sun angle, θ_S , completes a full revolution once every synodic period. For example, a pe-

riodic halo orbit in the Sun-Earth-Moon BCR4BP, that is computed about the Earth-Moon L_2 libration point, is displayed in Figure 3. This orbit possesses a

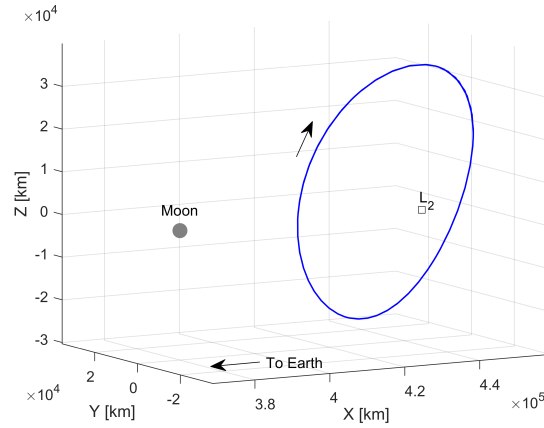


Fig. 3: 2:1 synodic resonance halo orbit in the Sun-Earth-Moon BCR4BP that is computed about the Earth-Moon L_2 libration point. This orbit is used as a staging orbit in the proposed design framework. Projected in the xy -plane of the Earth-Moon rotating frame.

2:1 synodic resonance, i.e., two revolutions along the halo orbit are completed for every one synodic period. Similarly, the individual trajectories along the invariant manifold associated with a periodic orbit in the BCR4BP are associated with unique Sun angles. Every path along a stable or unstable manifold arrives at or departs from the periodic orbit at a specific Sun angle. Structures available in the BCR4BP can appear similar to those in the CR3BP, but the dependency on Sun angle is critical.

2.3 Direct Collocation

Low-thrust trajectory design is frequently posed as a continuous optimal control problem; at each instant in time a thrust vector is selected that minimizes a cost, typically propellant consumption, time of flight, or some combination. A multitude of strategies for solving continuous optimal control problems are available, and the best strategy is dependent on the characteristics of the problem. In this investigation, a direct optimization technique is employed because these methods are generally more robust to poor initial guesses than indirect optimization formulations and require less computational time than global optimization approaches. This balance of robustness and efficiency is critical for the proposed de-

sign framework because it aims to rapidly explore a large search space of potential LIC trajectory solutions.

The process of discretizing a continuous optimal control problem to allow a numerical solution is denoted transcription, and collocation offers one approach to this procedure. A collocation scheme uses polynomials to approximate a solution to the set of differential equations that govern a dynamical model, for example, Equations (1)-(3). A collocation problem is discretized into n segments where the dynamics along each segment are approximated by a polynomial. Many collocation schemes are differentiated by the type and degree of polynomial used; this investigation employs 7th degree Legendre Gauss polynomials. Collocation is the transcription method of choice in this investigation due to its wide basin of convergence and amenability to the addition of constraints. Collocation often exhibits a wider basin of convergence than other approaches for solving a system of differential equations, i.e., it will converge upon a solution despite a poor initial guess, even when other methods fail. Since this investigation utilizes direct optimization, the overall optimization approach employed here is termed *direct collocation*.

The tool that implements direct collocation for this investigation is labelled COLT (Collocation with Optimization for Low-Thrust) and was developed in collaboration with Daniel Grebow at the Jet Propulsion Laboratory. The direct collocation framework in COLT generally follows the scheme developed by Grebow and Pavlak and implemented in their MColl software²⁶. This scheme is demonstrated to successfully solve many types of low-thrust trajectory design problems.²⁷⁻²⁹ Solution of this broad range of trajectory design scenarios is aided by the availability of a variety of problem constraints in COLT. While some constraints must be enforced to obtain a solution to the low-thrust trajectory optimization problem, others are only included for specific scenarios. For example, it is frequently beneficial to include minimum radius constraints with respect to gravitational bodies. This constraint enforces a “keep-out” zone around these bodies such that the trajectory remains beyond the zone. Other useful constraints include constraining the states, energy, and/or orbital elements for the initial and final boundary points along a trajectory arc. Specific low-thrust trajectory design scenarios may require other constraints, and these are straightforward to incorporate in a collocation framework.

Several additional features of COLT are available in the current version of the algorithm. The design

variable and constraint framework for implementing collocation is paired with the optimizer IPOPT³⁰ to compute mass optimal low-thrust trajectories. For a more tractable optimization problem, the design variables are frequently bounded within a desired range. Some design variables possess obvious upper and lower bounds; for example, necessary constraints on the control and mass variables are enforced simply by applying bounds. Bounds on other variables, such as the position and velocity states, are defined relative to their initial values and are defined as user inputs. Convergence to an optimal solution is also aided by the ability to scale the design variables and constraints. Finally, collocation is typically paired with a mesh refinement scheme to generate a sufficiently accurate solution. Mesh refinement schemes adjust the spacing of boundary points along a solution to evenly distribute and ultimately reduce error. The mesh refinement strategies leveraged in this investigation, developed by Grebow and Pavlak, are labelled Control Explicit Propagation (CEP) and Hybrid CEP.²⁶ Bounding the design variables, scaling the problem, and conducting mesh refinement ensure that COLT is a robust and efficient direct collocation algorithm.

2.4 Nearest Neighbor Search

The proposed trajectory design framework employs maps to aid the construction of initial guesses that are passed to the direct collocation algorithm. Maps capture the returns of trajectory segments to a particular hyperplane, Σ . Frequently, maps are used to facilitate the identification of close connections between two sections of a spacecraft trajectory, e.g., one propagated forward in time and the other backward. Points along these trajectories that intersect the selected hyperplane are displayed on the map. Example hyperplanes include a plane in configuration space, e.g., the xy -plane, or the occurrence of a specific epoch. In this investigation the Sun angle, θ_S , is used to define hyperplanes for two different maps. Parameters such as position, velocity, or energy at the hyperplane intersections may be displayed on the map. The maps in this analysis include points, i.e., hyperplane crossings, from many trajectories, and each trajectory can possess multiple returns to the hyperplane. Due to the large number of points and multiple dimensions of each point plotted on the map it can be challenging to visually identify the best connections between trajectory segments. Therefore, a nearest neighbor search algorithm aids the identification of points on maps that

share similar characteristics.

Nearest neighbor (NN) algorithms are employed in many computer science fields under a variety of names.³¹ Fundamentally, the nearest neighbor problem involves locating the point p in a set of points P with the shortest distance to a given point q , assuming all points occupy a space of dimension d .³² In the present application, events along the forward propagated group of trajectories provide one set of points, while events on the backward propagated trajectories comprise the other set. Thus, an NN search is ideally suited for identifying close connections between these two sets. The tool *Poincare*, developed at JPL, employs NN algorithms for this purpose.³³ In this investigation, Matlab's `knnsearch` algorithm is employed for the NN search. Furthermore, a standardized Euclidean distance metric is used to compute the distances between points. As NN search supplements visual identification of close connections on a map, only parameters visible on the map are included in the search. In this case, these parameters are x and y position in the Earth-Moon rotating frame, the value of the Hamiltonian, H , and the angle of the xy -plane projection of the velocity vector with respect to \hat{x} . Because these parameters can possess different magnitudes, the distance metric applies scaling to prevent one set of parameters from biasing the search. The standard deviations of each of the NN search parameters are used as scaling factors. If desired, the scaling factors may be weighted to emphasize close matches in specific parameters. This weighting is achieved by decreasing the value of the scaling factors for the parameters that are to be emphasized. The NN search algorithm is a useful tool that complements visual inspection of maps to identify close connections between trajectory segments.

3. TRAJECTORY DESIGN FRAMEWORK

The proposed trajectory design framework is distinguished by three key features: modeling in the BCR4BP, employing a staging orbit, and computing low-thrust transfers with direct collocation. Together, these design choices deliver a flexible and robust procedure for constructing the LIC trajectory. A staging orbit near the Moon is used to divide the mission design challenge into two phases, as illustrated in Figure 4. Phase 1 occurs from deployment to the staging orbit and Phase 2 passes from the staging orbit to the low lunar altitude science orbit. These two phases are solved nearly independently, where the spacecraft mass is the only parameter, aside from the selected staging orbit, carried over between phases.

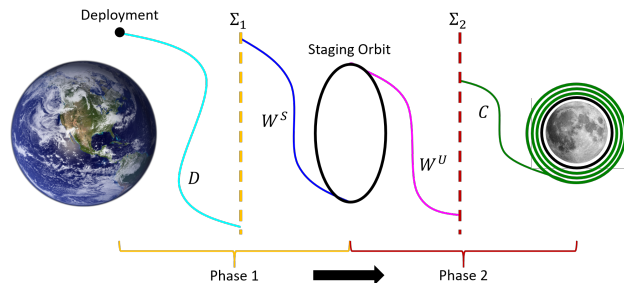


Fig. 4: Schematic of trajectory design framework.

In the BCR4BP, any discrepancies in epoch between the two phases are overcome simply by waiting in the staging orbit until the desired departure epoch is reached. Initial guesses for both phases of the trajectory design framework are assembled with the aid of two different maps. These maps display intersections with the hyperplanes Σ_1 and Σ_2 which are defined by the Sun angles θ_{S_1} and θ_{S_2} , respectively. The first map captures intersections of Σ_1 by forward propagated deployment trajectory arcs, D , and backward propagated paths on the stable manifold of the staging orbit, W^S . Similarly, the second map captures intersections of Σ_2 by forward propagated trajectories on the unstable manifold of the staging orbit, W^U , and backward propagated capture trajectory arcs, C . Close matches between hyperplane intersections of forward and backward propagated trajectories are identified and their corresponding trajectory segments are assembled into an initial guess for the direct collocation tool COLT.

3.1 Phase 1: Deployment to Staging Orbit

Design of Phase 1 of the LIC trajectory is facilitated by the creation of maps that display intersections of Σ_1 along trajectories propagated forward from deployment and backward on the stable invariant manifold of the staging orbit. To expand the options available on these maps, a range of D and W^S trajectory arcs are generated. Different W^S arcs are obtained by changing the state and epoch of the departure point from the periodic orbit. In contrast, because the deployment state and epoch cannot be changed, a span of D trajectory segments is generated by varying thrust direction prior to the first Lunar flyby. The deployment state and epoch used in this investigation are the same as those used to generate the baseline trajectory displayed in Figure 1.

Trajectories propagated forward in time from the deployment condition, D , are divided into three parts, an initial coast period, a thrust segment, and a

second coast period. An example of this subdivision is displayed in Figure 5. The duration of the first

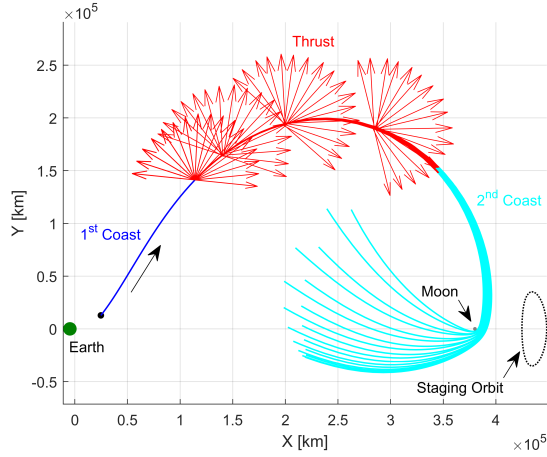


Fig. 5: Sample range for deployment trajectories in the creation of a Phase 1 map, plotted in the Earth-Moon rotating frame. The first coast period is 0.8 days, the thrust segment is 3 days, and the second coast section is 4 days. Thrust vectors span a range of α angle values from 0 to 270° in the VNB frame. Trajectories that impact the Moon are omitted.

coast segment is set to 0.8 days and is dictated by the time required to perform initial spacecraft systems checkouts and obtain tracking data. Following this coasting period, a multi-day thrust segment is introduced. A thrust segment of three days is used in this investigation; however, this value can be altered to change the post-flyby behavior of the deployment trajectory. The direction of the thrust vector along this segment is varied over a user-defined span of angles to generate a range of deployment trajectories. The angle, α , used to determine the thrust vector direction is defined relative to the \hat{v} unit vector in the velocity-normal-binormal (VNB) frame. This frame is defined such that the \hat{v} unit vector is in the direction of the velocity vector of the spacecraft expressed in the rotating frame. Additionally, the \hat{n} unit vector is in the direction of the spacecraft's angular momentum vector relative to B_1 , and the \hat{b} unit vector is defined to complete the orthonormal set. The angle α determines the direction of the thrust vector in the vb -plane, and no out-of-plane, i.e., \hat{n} component of the thrust vector, is introduced. By varying α from α_{min} to α_{max} many different post-flyby trajectories are generated, as seen in Figure 5. In this investigation, $\alpha_{min} = 0$ and $\alpha_{max} = 270^\circ$. Following

the thrust segment, a second coast segment is propagated for a user-defined number of days. Intersections of these D trajectory arcs with the hyperplane Σ_1 are recorded and used to generate the map.

The forward propagated D trajectory arcs are linked to trajectories propagated backward in time along the stable manifold, W^S , of the staging orbit. The stable invariant manifolds of periodic orbits offer efficient paths onto the orbits. Thus, using these trajectories to guide LIC to the staging orbit should lead to a solution that requires less propellant than other potential insertion paths. Figure 6 displays trajectories along the stable manifold. The initial trend of

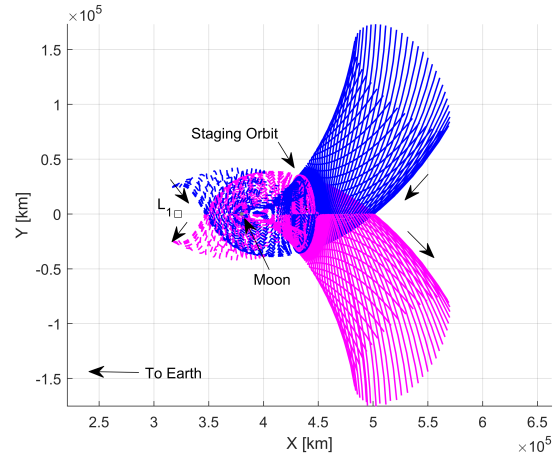


Fig. 6: Stable (blue) and unstable (magenta) manifold trajectories plotted in the Earth-Moon rotating frame and originating from the 2:1 resonant L_2 halo orbit displayed in Figure 3.

these manifold paths is either in the positive or negative x direction. In the former case, trajectories on the manifold tend to escape the Earth-Moon system, and these paths offer more useful connection points with the D trajectory arcs. Stepping off the periodic orbit and onto the stable manifold at different states and epochs around the orbit generates a variety of manifold paths.

A map is created to join the two halves of the Phase 1 LIC trajectory by recording intersections of the D and W^S trajectory arcs with Σ_1 . Trajectories are propagated until either a maximum time limit or a maximum distance from the Earth is reached. In this case, a maximum time of 100 days and a maximum Earth distance of 3×10^6 km are used for both the D and W^S propagation. An example map is displayed in Figure 7 where the Sun angle at which events are recorded is $\theta_{S_1} = 135^\circ$. The events that oc-

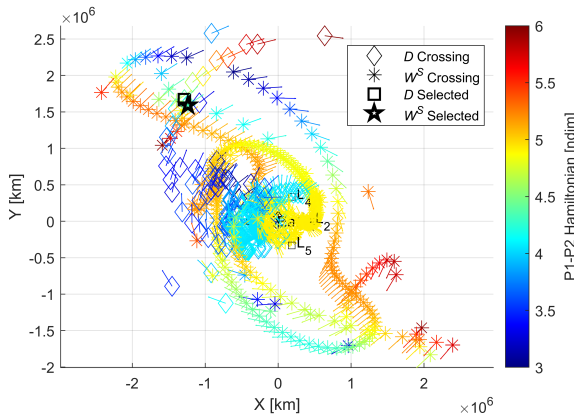


Fig. 7: Map of Σ_1 intersections of the forward propagated D and backward propagated W^S trajectory arcs in the BCR4BP. Intersections are projected in the xy -plane of the Earth-Moon rotating frame, and the Sun angle selected for Σ_1 is $\theta_{S_1} = 135^\circ$.

cur along the D trajectories are plotted as diamonds, while the events on the W^S arcs are marked as asterisks. All events are plotted in the Earth-Moon rotating frame, and each marker is colored according to the Hamiltonian, H , of the spacecraft at the time of the event. Additionally, the spacecraft's xy -plane velocity direction is plotted as an arrow centered at the marker. Adding this extra information to each plot aids the identification of close matches between D and W^S trajectories. By selecting intersections that match closely in position space along with energy and velocity direction, useful initial guesses for the direct collocation algorithm can be obtained. A close match, identified by the nearest neighbor algorithm, is highlighted in Figure 7. The D and W^S trajectories are propagated to the selected intersection times and used as an initial guess for the direct collocation algorithm in the Sample Trajectory Design section.

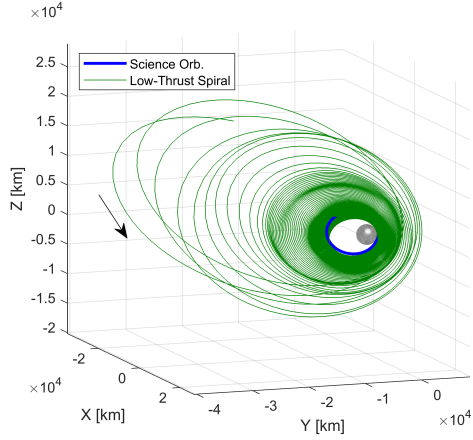
3.2 Phase 2: Staging Orbit to Science Orbit

Phase 2 of the LIC trajectory consists of the transfer from the staging orbit to the science orbit. An initial guess for this phase is assembled in a similar manner to Phase 1; intersections with Σ_2 , along a range of forward and backward propagated trajectories, are plotted on a map used to select the initial guess. In this case, paths along the unstable manifold, W^U , of the staging orbit make up the forward propagated trajectory segments. The backward propagated seg-

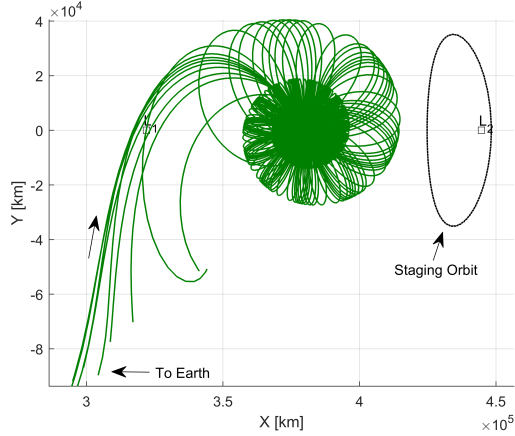
ments, C , consist of trajectories propagated with low-thrust, in reverse time, from different true anomaly values on the science orbit. The map used to link the forward and backward propagated trajectories consists of intersections with Σ_2 , defined by the Sun angle θ_{S_2} , along these trajectory segments.

Trajectories along the unstable manifold, W^U of the staging orbit offer energy efficient paths for departing the orbit and beginning the spiral down to the science orbit. Apart from their inverse direction, these trajectories behave similarly to those on the stable manifold and are displayed in Figure 6. Paths on W^U offer a variety of locations and epochs at which to depart the staging orbit, and intersections with Σ_2 along these trajectories populate the Phase 2 map.

To generate a variety of C trajectories that insert onto the final orbit, backward propagation is initiated from true anomaly values on the orbit that span the full 360° range. The backward propagation assumes a maximum thrust anti-velocity control law - that is, the thrust vector is always oriented along the $-\hat{v}$ direction of the VNB frame and has a magnitude equal to the maximum thrust of LIC. Recall that the VNB frame is defined relative to the rotating frame velocity vector. Application of this control law produces a trajectory that, in forward time, gradually spirals down to the final science orbit, as shown in Figure 8(a). The C trajectory arcs must assume an epoch for insertion onto the science orbit as well as a spacecraft mass at insertion. Reasonable inferences for these values made during initial guess formulation are later adjusted by the direct collocation algorithm to ensure a continuous final result. Previous analyses have indicated that the total duration of the LIC transfer is approximately one year, thus a date of June 1st, 2021 is used to obtain a Sun angle at science orbit insertion (SOI) of 105.7° . Similarly, earlier investigations indicate that, at most, LIC consumes half of the available propellant mass to execute the transfer from deployment to science orbit, therefore a final mass at SOI of 13.25 kg is assumed. Even if an intuition for the epoch and mass at SOI is not available, the robustness of the direct collocation algorithm increases the likelihood that poor estimates for these values can still produce useful initial guesses. While these two quantities are constant for all backward propagated trajectories, using a range of true anomaly values to initialize propagation ensures that each trajectory evolves differently, as seen in Figure 8(b). Trajectories are propagated until either a maximum time limit or a maximum distance from the Earth is reached. In this case, W^U arcs are propa-



(a) Single backward propagated trajectory in the Moon-centered J2000 inertial frame.



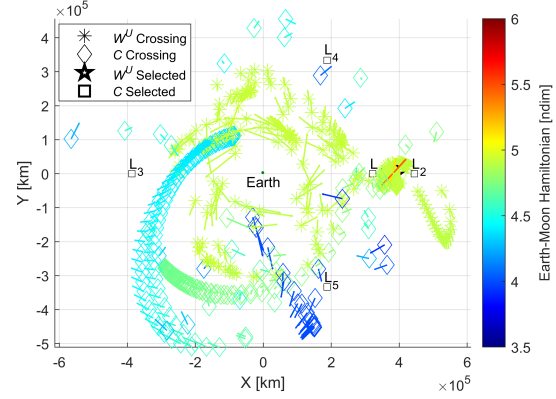
(b) Multiple backward propagated trajectories in the Earth-Moon rotating frame generated by initiating propagation at different true anomaly values on the science orbit.

Fig. 8: Backward propagation from the science orbit with a constant maximum thrust anti-velocity thrust vector.

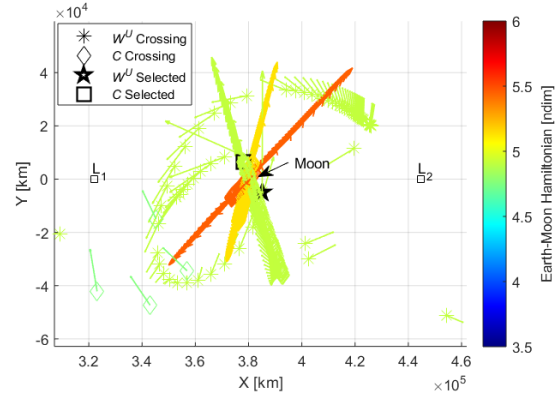
gated for a maximum time of 100 days while C trajectory segments are propagated up to 200 days. Both types of trajectories are propagated to a maximum distance from the Earth of 6×10^5 km. Intersections with Σ_2 along each propagated trajectory are recorded and added to the Phase 2 map.

Intersections with Σ_2 along the W^U and C trajectory segments generated for Phase 2 are projected on the xy -plane and colored according to their H value. These three parameters, along with the in-plane direction of the velocity vector, are used to identify close matches between trajectory segments. An example map is displayed in Figure 9(a) where the Sun

angle that defines Σ_2 is $\theta_{S_2} = 75^\circ$. The intersections



(a) Earth-Moon Rotating Frame



(b) Phase 2 Map

Fig. 9: Map of Σ_2 intersections of the forward propagated W^U and backward propagated C trajectory arcs in the BCR4BP. Intersections are projected in the xy -plane of the Earth-Moon rotating frame, and the Sun angle selected for Σ_2 is $\theta_{S_2} = 75^\circ$.

that occur along the C arcs are plotted as diamonds, while those on the W^U paths are displayed as asterisks. A close match, identified by the nearest neighbor algorithm, is highlighted in Figure 9(b). The deployment and manifold trajectories propagated to the selected intersection times are used as an initial guess for the direct collocation algorithm in Section 4.

Modifications are made to COLT's nominal collocation scheme to enable design of a continuous low-thrust transfer from the staging orbit to the final science orbit for LIC. The low-thrust spiral required to transfer between these two orbits is long and includes

many revolutions. This type of trajectory is challenging to optimize using the collocation framework implemented in COLT, which employs Cartesian coordinates. Other collocation schemes that utilize modified equinoctial elements (MEE) have successfully optimized low-thrust spiral trajectories.^{34,35} However, rather than implement a complex multi-phase collocation scheme that uses Cartesian and MEE coordinates, a simplified approach is used. This strategy divides Phase 2 into two halves: one is solved with direct collocation and the other is explicitly propagated backward in time from science orbit insertion (SOI).

The backward propagated section of the LIC trajectory is updated in the direct optimization process by the addition of three design variables and a constraint. The three design variables govern: the backward propagation time from SOI, the true anomaly value on the science orbit at insertion, and the spacecraft mass at SOI. By including these variables in the corrections process, the evolution of the spiraling LIC trajectory is allowed to change and can be joined with the section of the transfer that departs from the staging orbit. A constraint is added to ensure state and mass continuity between these two halves of the LIC trajectory. With the addition of the three design variables and constraint, a single direct collocation problem is solved to generate a continuous low-thrust transfer from the staging to the science orbit. Because a sub-optimal control law is used for the spiraling portion of the trajectory, the result of the direct collocation algorithm is not a fully optimized low-thrust transfer. However, optimization is used to minimize the propellant consumed before the explicitly propagated spiraling phase begins. Additionally, as the selected control law ensures the maximum rate of change of the spacecraft's energy, and this reduces the time required to achieve Lunar capture, propellant consumption is reduced. This approach for computing a trajectory from the staging to the science orbit generates a continuous low-thrust transfer without the complexity of a multi-phase collocation scheme.

4. SAMPLE TRAJECTORY DESIGN

The proposed trajectory design framework offers a procedure for developing an initial guess for the full Lunar IceCube trajectory, from deployment to insertion on the science orbit. After maps are generated for Phases 1 and 2, close matches between forward and backward propagated trajectory segments are identified and used to construct an initial guess

for the direct collocation algorithm. This robust algorithm is frequently able to converge even when given very discontinuous initial guesses.

4.1 Phase 1: Deployment to Staging Orbit

An initial guess for Phase 1 of the Lunar IceCube trajectory is assembled by identifying a close match between Σ_1 intersections on D and W^S trajectories in a Phase 1 map. An example of such a match is highlighted by black markers in Figure 7, where the black square indicates the deployment event and the black five-pointed star denotes the manifold event. This match is identified using the NN search algorithm and the trajectories that correspond to the selected events are shown in Figure 10. While a discontinu-

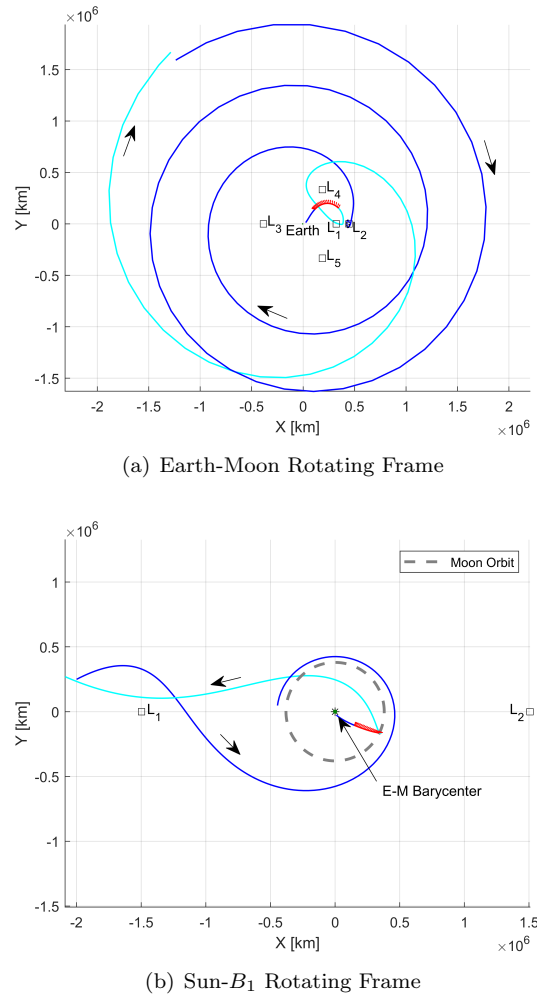
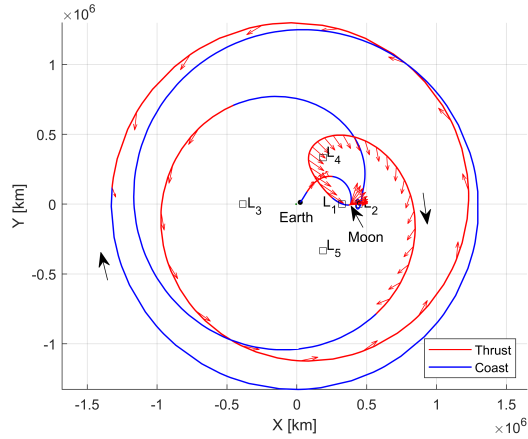
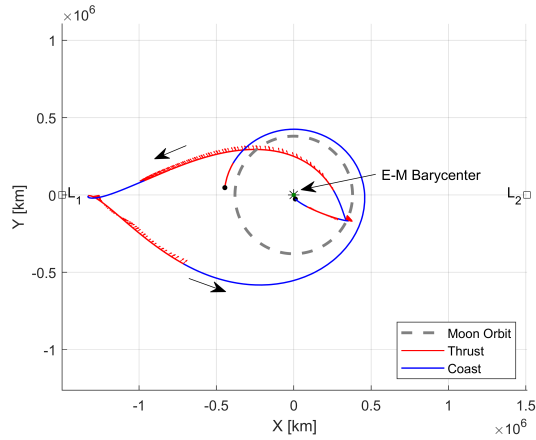


Fig. 10: Initial guess for Phase 1 trajectory. Corresponds to the match identified in the Phase 1 map created with $\theta_{S_1} = 135^\circ$ displayed in Figure 7.

ity between the forward and backward propagated trajectories is evident, the criteria used to identify matches between Σ_1 crossings on the map yield a promising initial guess. This initial guess is passed to COLT, which eliminates the discontinuity by inserting additional thrust segments. The optimized trajectory resulting from this initial guess is displayed in Figure 11, and consumes 0.23 kg of propellant to reach the staging orbit in 140 days. The collocation



(a) Earth-Moon Rotating Frame

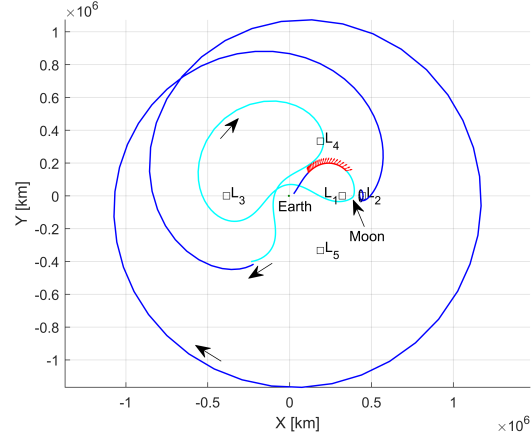


(b) Sun- B_1 Rotating Frame

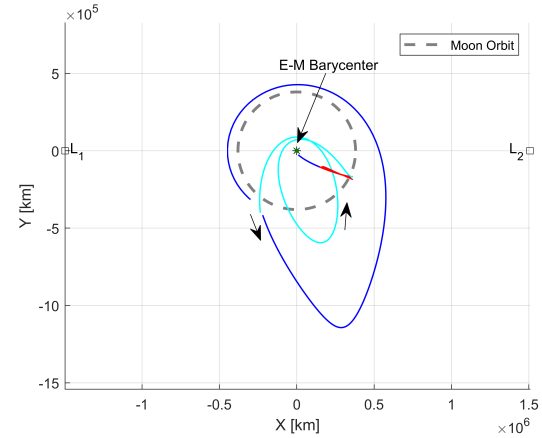
Fig. 11: Direct collocation result for Phase 1 transfer using the initial guess in Figure 10. This transfer requires 140 days and 0.23 kg of propellant.

algorithm computes this solution with relatively few iterations; moreover, the geometry of the initial guess is generally preserved in the direct collocation result. These two factors indicate that the initial guess identified with the Phase 1 map was useful in guiding the algorithm towards a solution.

The strong influence of the initial guess on the final result is more evident when alternate solutions are examined. A different Phase 1 map, one generated with $\theta_{S_1} = 180^\circ$, is used to construct the initial guess shown in Figure 12. This initial guess includes



(a) Earth-Moon Rotating Frame



(b) Sun- B_1 Rotating Frame

Fig. 12: Initial guess for Phase 1 trajectory that includes an Earth flyby. Corresponds to a close match identified in a Phase 1 map at $\theta_{S_1} = 180^\circ$.

an Earth flyby, and this flyby is maintained in the optimized COLT solution displayed in Figure 13. This transfer reaches the staging orbit in approximately 115 days and requires 0.27 kg of propellant mass. By experimenting with maps generated using different values of θ_{S_1} and selecting various crossing pairs on those maps, a variety of initial guess geometries can be obtained that lead to an array of optimized solutions. The flexibility of this approach and the diversity of solutions it offers makes it adaptable to

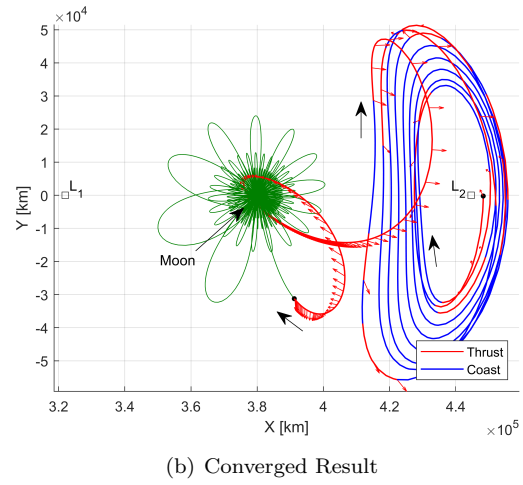
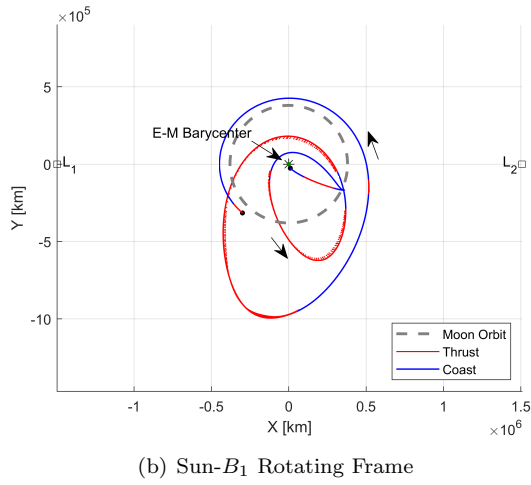
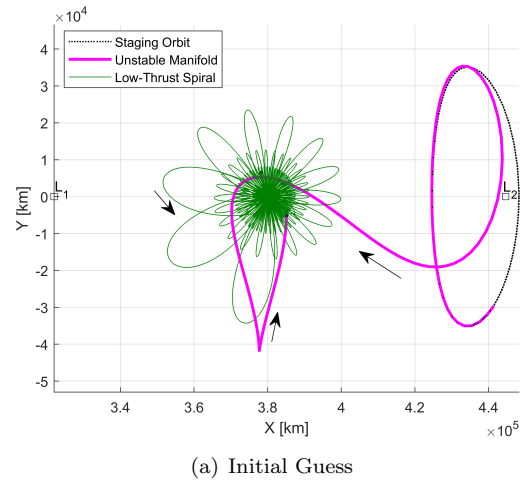
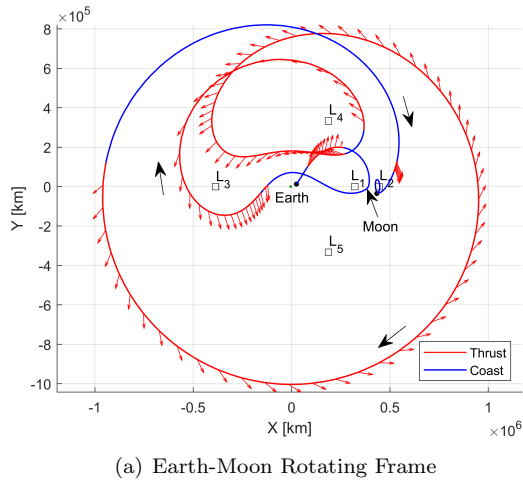


Fig. 13: Direct collocation result for Phase 1 transfer using the initial guess in Figure 12. This transfer requires 115 days and 0.27 kg of propellant.

Fig. 14: Initial guess and direct collocation result for Phase 2 transfer in the Earth-Moon rotating frame that remains in the Lunar vicinity. The initial guess corresponds to the close match identified in the Phase 2 map at $\theta_{S_2} = 75^\circ$ displayed in Figure 9. The resulting transfer requires 228 days and 0.52 kg of propellant.

different mission constraints and deployment conditions.

4.2 Phase 2: Staging Orbit to Science Orbit

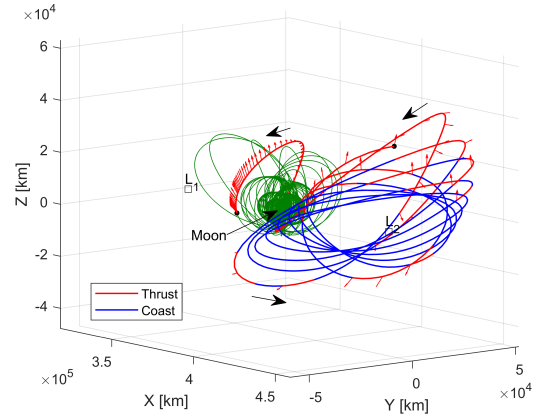
A solution for Phase 2 of the LIC trajectory is computed in a similar manner to Phase 1, and because a staging orbit is used, little information on the converged results of Phase 1 is required to develop an initial guess for Phase 2. A close match between Σ_2 crossings on a sample Phase 2 map is identified in Figure 9, and the trajectories corresponding to the selected intersections are displayed in Figure 14(a). Because the staging orbit and the science orbit are significantly out-of-plane, the xy -plane view of the Phase 2 map shown in Figure 9 can be deceptive.

Events that appear to overlap in this map may differ significantly when the \hat{z} position and velocity components are considered. As a result, the NN search is especially useful for identifying matches on the Phase 2 map, because the algorithm can be weighted to emphasize close matches in energy, a parameter that includes information on the out-of-plane components of each event. The close connection point between the unstable manifold and low-thrust spiral trajectories displayed in Figure 14(a) actually occurs under the Moon, i.e., $z < 0$, making it is difficult to see, even

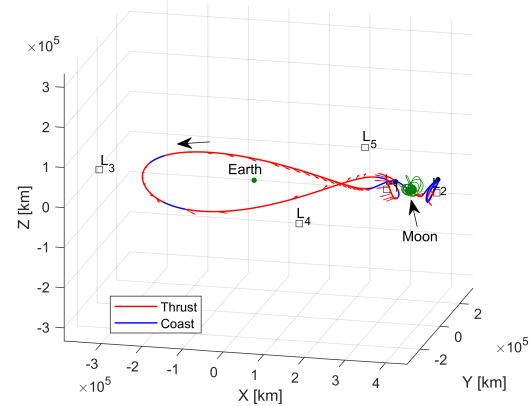
in the zoomed in view of the Phase 2 map shown in Figure 9(b). Utilizing the NN algorithm ensures that this close match is not overlooked.

The initial guess identified in Figure 9 is passed to the direct collocation algorithm, COLT, for convergence. In general, it is more difficult to achieve convergence for this phase of the LIC trajectory because the initial guesses generated by the map possess larger state discontinuities and the majority of the trajectory is near the Moon, which increases the sensitivity of the optimizer. The likelihood of convergence is increased by bounding the design variables, scaling, and including a minimum radius constraint with respect to the Moon. Additionally, convergence is improved by providing COLT more trajectory, and therefore more time, with which to achieve the desired transfer. This is done by “stacking” additional revolutions of the staging orbit prior to departure on the unstable manifold path.²⁸ Four additional revolutions on the staging orbit are added to the initial guess displayed in Figure 14(a). Thus, the initial guess passed to COLT consists of these four revolutions, the unstable manifold trajectory, and the backward propagation parameters, i.e., the three additional design variables, that produce the low-thrust spiral displayed in Figure 14(a). With this initial guess, COLT computes the low-thrust transfer in Figure 14(b), which requires approximately 228 days and 0.52 kg of propellant to achieve. The solution displayed in Figure 14(b) shows that the stacked staging orbit revolutions included in the initial guess are distributed by the direct collocation algorithm into a quasi-periodic-like structure. This new motion is even more evident in Figure 15(a), a three-dimensional view of the transfer. After moving along this structure, the spacecraft departs the vicinity of the staging orbit and conducts a powered lunar flyby to insert on the explicitly propagated low-thrust spiral trajectory. This geometry is influenced by the initial guess, which also includes an unstable manifold trajectory with a close lunar flyby.

Several important differences exist between the convergence process for Phase 1 and 2 transfers. First, the initial mass used to converge a Phase 2 transfer must be the final mass of a converged Phase 1 transfer. In this case, the final mass of the transfer shown in Figure 11 is used as the initial mass for the transfer in Figure 14(b). The spacecraft mass is the only parameter from Phase 1 that must be carried over to compute Phase 2. Furthermore, the spacecraft mass and the maximum thrust, T_{max} , determine the maximum acceleration that the spacecraft can



(a) Near Moon Transfer



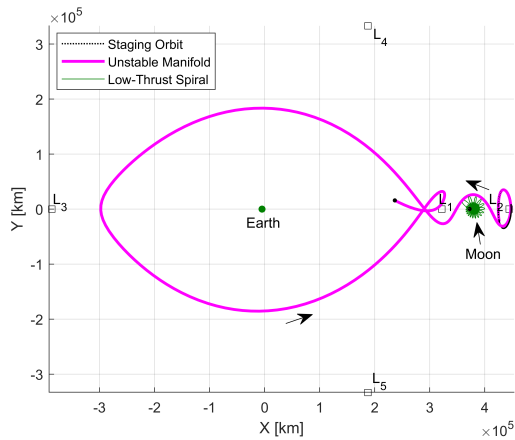
(b) Around Earth Transfer

Fig. 15: Out-of-plane views in the Earth-Moon rotating frame of two Phase 2 transfer options.

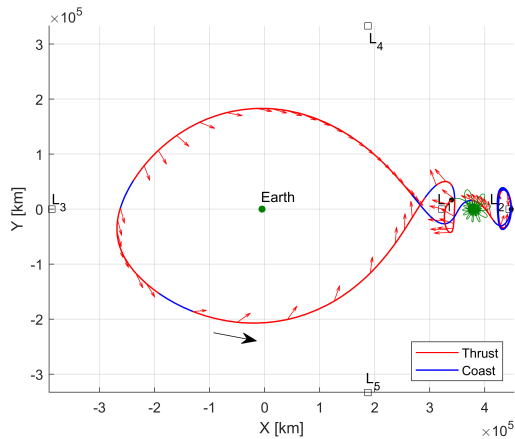
produce. When convergence difficulty is encountered, it is frequently advantageous to temporarily raise the maximum available acceleration by first computing a transfer that uses a T_{max} value marginally higher than that available to LIC. Then, a natural parameter continuation process can be used to lower T_{max} to the correct value. Continuation is employed to obtain both of the staging to science orbit transfers presented in this investigation. Finally, as stated previously, because the low-thrust spiral phase of the staging to science orbit transfer is explicitly propagated with a sub-optimal control law, the resulting transfer is not fully optimal. Instead, the objective of the direct collocation problem in this phase is to maximize the mass at the connection point between the trajectory computed with collocation and the ex-

plicitly propagated low-thrust spiral.

Phase 2 transfers generally fall into one of two categories: transfers that remain near the Moon, as seen already, and those that include at least one loop around the Earth. The latter of these two options is examined by generating a new Phase 2 map. A close connection is identified on a Phase 2 map generated with Σ_2 defined by a Sun angle of $\theta_{S_2} = 315^\circ$, and the resulting initial guess is displayed in Figure 16(a). In this case, the difference in position between



(a) Initial Guess



(b) Converged Result

Fig. 16: Initial guess and direct collocation result for Phase 2 transfer in the Earth-Moon rotating frame that includes a loop around the Earth. The initial guess corresponds to a close match identified in a Phase 2 map at $\theta_{S_2} = 315^\circ$. The resulting transfer requires 212 days and 0.52 kg of propellant.

the end of the unstable manifold trajectory and the

beginning of the low-thrust spiral is especially large. However, these two points are relatively close in energy and in velocity direction. Thus, the NN search algorithm identifies this initial guess that may have been disregarded by a visual inspection. Despite the seemingly large discontinuity, COLT uses this initial guess to compute the low-thrust transfer shown in Figure 16(b). This transfer delivers the spacecraft from the staging orbit to the science orbit in 212 days and requires roughly the same propellant mass as the previous case, 0.52 kg. Figures 15(b) and 16(b) illustrate that rather than using repeated revolutions near the staging orbit, much of the plane change required to begin the spiral down to the science orbit is completed during the transit around the Earth. This behavior, and the lack of a low-altitude Lunar flyby, make this transfer and others like it easier to converge because the larger distance from the Moon decreases the sensitivity of the optimization problem.

Combining the results computed for Phases 1 and 2 of the LIC trajectory yields complete deployment to science orbit trajectories. The sample LIC trajectories computed in the BCR4BP using the proposed framework are summarized in Table 3. The Phase 1 transfer without an Earth flyby, shown in Figure 11, is labeled A while the transfer that includes the Earth flyby, displayed in Figure 13, is B. Similarly, the Phase 2 transfer that remains near the Moon, depicted in Figure 14(b), is labeled C and the transfer that loops around the Earth, shown in Figure 16(b), is D. Note that for all transfer combinations, up to a month of additional transfer time is added to account for the phasing time that must be included in the staging orbit following Phase 1 of the transfer. This time allows the spacecraft to reach the state and Sun angle required to begin Phase 2. In this case, the maximum phasing time required is 25 days and the minimum is 0.5 days. Over a third of the total time of flight (TOF) is spent in the transfer from the staging orbit to the beginning of the low-thrust spiral, and a quarter of the TOF is occupied by the subsequent spiral. In total, all four transfers reach the science orbit about one year after deployment.

The final mass of all four transfer combinations in Table 3 is nearly the same. This similarity is likely a result of the initial guess used for the mass at SOI, m_{SOI} , in the Phase 2 map generation process. In this case, $m_{SOI} = 13.25$ kg, so while m_{SOI} is a variable in the direct collocation algorithm, the value of this quantity is only altered enough to achieve continuity. One approach for overcoming the bias of the initial guess is to set the maximization of m_{SOI} as the ob-

jective of the direct collocation problem. However, the sensitivity of the problem to this variable makes achieving convergence difficult when m_{SOI} is used as the objective. Instead a higher initial mass at SOI may be achieved by iterating the value of the initial guess for m_{SOI} employed in the Phase 2 map generation process. To do this, a higher value of m_{SOI} is used to generate new Phase 2 maps then the process of assembling and converging an initial guess is repeated. Changes in m_{SOI} affect the rate of change of LIC's energy, however the behavior of the low-thrust spiral is not significantly different. Thus, similar initial guesses can be found as m_{SOI} is iterated by changing the value of θ_{S_2} at which Phase 2 maps are generated. A process of iterating the estimated value of m_{SOI} for the Phase 2 transfer can be used to increase the mass delivered to the science orbit. Ultimately, this procedure reaches a limit where no transfers with higher m_{SOI} values can be computed.

The transfer times and propellant consumption values provided in Table 3 are comparable to the current baseline trajectory shown in Figure 1. While the transfers computed with the proposed framework all require more time and propellant than the baseline, several steps are available that may reduce the time and change in mass of these transfers. First, an iterative process of estimating successively higher values for m_{SOI} can be undertaken, as described previously. Second, while the additional staging orbit revolutions added to the initial guess for Phase 2 are useful to achieve convergence, it may be possible to remove some of them after a transfer is converged. For example, some of the revolutions near the staging orbit that appear in Figure 15(a) could likely be removed because they consist largely of long coast segments. If possible, removing excess trajectory will reduce transfer time. Finally, using a multi-stage collocation algorithm to solve Phase 2 will offer the greatest improvement in delivered mass because the majority of propellant consumption occurs in this phase. A multi-stage approach would permit the low-thrust spiral to the science orbit to be fully optimized, thereby increasing m_{SOI} . These three steps can lead to reductions in both time of flight and propellant consumption for the LIC transfer.

5. CONCLUDING REMARKS

The proposed framework for constructing a LIC baseline trajectory addresses the need for a design methodology that is both robust and flexible. Employing a dynamical model that includes the Sun enables the perturbing acceleration of this body to be

Table 3: Summary of sample transfers. All results are from the given deployment state to the science orbit. Given characteristics are time of flight (TOF), mass at science orbit insertion (m_{SOI}), and total change in mass (Δm).

Transfer	TOF [days]	m_{SOI} [kg]	Δm [kg]
A \rightarrow C	369.25	13.25	0.75
B \rightarrow C	369.63	13.25	0.75
A \rightarrow D	353.02	13.24	0.76
B \rightarrow D	323.50	13.24	0.76
Baseline	318	13.31	0.69

leveraged to achieve the desired transfer despite LIC's limited control authority. Moreover, utilizing direct collocation to converge initial guesses developed in the BCR4BP allows a wider range of guesses to be used due to the robustness of this algorithm. Flexibility is further enhanced by using a staging orbit to separate the LIC trajectory into two halves that can be designed independently. Together, these design choices offer a framework to systematically generate a variety of transfer configurations with time of flight and propellant consumption values comparable to the current baseline. Further improvements to this procedure could increase the efficiency of the process, enhance the quality of the solutions it generates, and broaden its applicability to missions beyond LIC.

ACKNOWLEDGEMENTS

The authors thank the Purdue University School of Aeronautics and Astronautics for facilities and support, including access to the Rune and Barbara Eliassen Visualization Laboratory. Additionally, many thanks to the members of the Purdue Multi-Body Dynamics Research Group for interesting discussions and ideas. Special thank you to Nicholas LaFarge for the idea of employing a nearest neighbor search algorithm and for guidance on its implementation. This research is supported by NASA Space Technology Research Fellowship, NASA Grant NNX16AM42H. Some analysis was conducted at the NASA Goddard Space Flight Center.

REFERENCES

- [1] J. Schoolcraft, A. T. Klesh, and T. Werne. MarCO: Interplanetary Mission Development On a CubeSat Scale. In *SpaceOps 2016 Confer-*

- ence, SpaceOps Conferences. American Institute of Aeronautics and Astronautics, May 2016.
- [2] P. Clark, B. Malphrus, R. MacDowall, D. C. Folta, A. Mandell, C. Brambora, D. Patel, S. Banks, K. Hohman, V. Hruby, K. Brown, J. Kruth, and R. Cox. Lunar Ice Cube: Determining Volatile Systematics Via Lunar Orbiting Cubesat. *European Planetary Science Congress*, 10:EPSC2015–61, Oct 2015.
- [3] A. J. Mazarr and D. C. Folta. Low-Thrust Station-Keeping for a Highly Elliptical Polar Orbit at the Moon. In *AAS/AIAA Astrodynamics Specialist Conference*, pages 1–31, Snowbird, Utah, 2018.
- [4] *BIT-3 RF Ion Thruster*. Busek Space Propulsion and Systems, 2019.
- [5] M. D. Rayman, P. Varghese, D. H. Lehman, and L. L. Livesay. Results from the Deep Space 1 Technology Validation Mission. *Acta Astronautica*, 47(2-9):475–487, 2000.
- [6] C. Russell and C. Raymond, editors. *The Dawn Mission to Minor Planets 4 Vesta and 1 Ceres*. Springer-Verlag, New York, 1 edition, 2012. ISBN 978-1-4614-4902-7.
- [7] S. L. Mccarty, L. M. Burke, and M. L. Mcguire. Analysis of Cislunar Transfers From a Near Rectilinear Halo Orbit With High Power Solar Electric Propulsion. In *AAS Astrodynamics Specialists Conference*, pages 1–14, Snowbird, UT, 2018.
- [8] R. Mathur. Low Thrust Trajectory Design and Optimization: Case Study of a Lunar CubeSat Mission. In *6th International Conference on Astrodynamics Tools and Techniques*, pages 1–11, Darmstadt, Germany, 2016. Emergent Space Technologies, Inc.
- [9] N. Bosanac. *Leveraging Natural Dynamical Structures to Explore Multi-Body Systems*. Ph.D. Dissertation, Purdue University, 2016.
- [10] N. Bosanac, A. D. Cox, K. C. Howell, and D. C. Folta. Trajectory design for a cislunar cubesat leveraging dynamical systems techniques: The lunar icecube mission. In *27th AAS/AIAA Space Flight Mechanics Meeting*, San Antonio, Texas, February 2017.
- [11] N. Bosanac, A. D. Cox, K. C. Howell, and D. C. Folta. Trajectory design for a cislunar CubeSat leveraging dynamical systems techniques: The Lunar IceCube mission. *Acta Astronautica*, 144: 283–296, 2018.
- [12] D. C. Folta, N. Bosanac, A. D. Cox, and K. C. Howell. The lunar icecube mission design: Construction of feasible transfer trajectories with a constrained departure. *Advances in the Astronautical Sciences*, 158:1369–1387, 2016.
- [13] W. S. Koon, M. W. Lo, J. E. Marsden, and S. D. Ross. Low energy transfer to the moon. *Celestial Mechanics and Dynamical Astronomy*, 81(1):63–73, 2001.
- [14] G. Gómez, W. Koon, M. Lo, J. Marsden, J. Masdemont, and S. Ross. Invariant manifolds, the spatial three-body problem and space mission design. *Advances in the Astronautical Sciences*, 109:3–22, 2002.
- [15] J. Parker and M. Lo. Shoot the moon 3d. *Advances in the Astronautical Sciences*, 123:2067–2086, 2006.
- [16] G. Mingotti, F. Topputo, and F. Bernelli-Zazzera. Low-energy, low-thrust transfers to the Moon. *Celestial Mechanics and Dynamical Astronomy*, 105(1):61–74, 2009.
- [17] A. Zanzottera, G. Mingotti, R. Castelli, and M. Dellnitz. Intersecting invariant manifolds in spatial restricted three-body problems: Design and optimization of Earth-to-halo transfers in the Sun-Earth-Moon scenario. *Communications in Nonlinear Science and Numerical Simulation*, 17(2):832–843, 2012.
- [18] P. J. Enright and B. A. Conway. Discrete Approximations to Optimal Trajectories Using Direct Transcription and Nonlinear Programming. *Journal of Guidance, Control, and Dynamics*, 15(4):994–1002, 1992.
- [19] D. J. Grebow, M. T. Ozimek, and K. C. Howell. Design of Optimal Low-Thrust Lunar Pole-Sitter Missions. *The Journal of Astronautical Sciences*, 58(1):55–79, 2011.
- [20] D. Pérez-Palau and R. Epenoy. Fuel optimization for low-thrust EarthMoon transfer via indirect optimal control. *Celestial Mechanics and Dynamical Astronomy*, 130(2):1–29, 2018.
- [21] R. L. Parker Jeffrey S.; Anderson. *Low-Energy Lunar Trajectory Design*. Deep Space Communications and Navigation Systems, Jet Propulsion Laboratory, Pasadena, California, 2013.
- [22] G. Mingotti, F. Topputo, and F. Bernelli-Zazzera. Efficient invariant-manifold, low-thrust planar trajectories to the Moon. *Communications in Nonlinear Science and Numerical Simulation*, 17(2):817–831, 2012.
- [23] Y. Cheng, G. Gómez, J. J. Masdemont, and J. Yuan. Study of the transfer between libration point orbits and lunar orbits in EarthMoon system. *Celestial Mechanics and Dynamical As-*

- tronomy*, 128(4):409–433, 2017.
- [24] P. Cao, B. He, and H. Li. Analysis of direct transfer trajectories from LL2 halo orbits to LLOs. *Astrophysics and Space Science*, 362(9), 2017.
 - [25] K. K. Boudad. Disposal Dynamics From The Vicinity Of Near Rectilinear Halo Orbits In The Earth-Moon-Sun System. Master’s Thesis, Purdue University, 2018.
 - [26] D. J. Grebow and T. A. Pavlak. MColl: Monte Collocation Trajectory Design Tool. In *AAS/AIAA Astrodynamics Specialist Conference*, Stevenson, Washington, 2017.
 - [27] R. E. Pritchett, K. C. Howell, and D. J. Grebow. Low-Thrust Transfer Design Based on Collocation Techniques: Applications in the Restricted Three-Body Problem. In *AAS/AIAA Astrodynamics Specialist Conference*, Stevenson, Washington, 2017.
 - [28] R. E. Pritchett, E. Zimovan, and K. C. Howell. Impulsive and Low-Thrust Transfer Design Between Stable and Nearly-Stable Periodic Orbits in the Restricted Problem. In *2018 AIAA/AAS Space Flight Mechanics Meeting*, Orlando, Florida, 2018. ISBN 978-1-62410-533-3.
 - [29] R. Pritchett, A. D. Cox, K. C. Howell, D. C. Folta, and D. Grebow. Low-Thrust Trajectory Design Via Direct Transcription Leveraging Structures from the Low-Thrust Restricted Problem. In *69th International Astronautical Congress*, pages 1–16, Bremen, Germany, 2018.
 - [30] A. Wachter and L. T. Biegler. On the Implementation of a Primal-Dual Interior Point Filter Line Search Algorithm for Large-Scale Nonlinear Programming. *Mathematical Programming*, 106(1):25–57, 2006.
 - [31] G. Shakhnarovich, P. Indyk, and T. Darrell. Introduction. In *Nearest-Neighbor Methods in Learning and Vision*, chapter 1, pages 1–12. MIT Press, Cambridge, Massachusetts, 1 edition, 2005.
 - [32] K. L. Clarkson. Nearest-Neighbor Searching and Metric Space Dimensions. In *Nearest-Neighbor Methods in Learning and Vision*, chapter 2, pages 15–59. MIT Press, Cambridge, Massachusetts, 1 edition, 2005.
 - [33] M. Vaquero and J. Senent. Poincare : A Multi-Body, Multi-System Trajectory Design Tool. In *7th International Conference on Astrodynamics Tools and Techniques*, pages 1–12, Oberpfaffenhofen, Germany, 2018.
 - [34] R. D. Falck, N. Glenn, and J. W. Dankanich. Optimization of Low-Thrust Spiral Trajectories by Collocation. In *AIAA/AAS Astrodynamics Specialist Conference*, pages 1–17, Minneapolis, Minnesota, 2012.
 - [35] Z. P. Olikara. Framework for Optimizing Many-Revolution Low-Thrust Transfers. In *AAS Astrodynamics Specialists Conference*, pages 1–19, Snowbird, Utah, 2018.